Self-Healing Thin Film Transistor Circuits on Flexible Substrates

Li Ding, Pushkaraj Joshi, James Macdonald, Virendra Parab and Sanjiv Sambandan*

Li Ding, Dr. Pushkaraj Joshi, Prof. Sanjiv Sambandan
Nanoscience Centre, Department of Engineering, University of Cambridge, 11 JJ Thomson
Ave, Cambridge CB30FF, UK
E-mail: ss698@cam.ac.uk

James Macdonald
Institute for Manufacturing, Department of Engineering, University of Cambridge, 17 Charles
Babbage Road, Cambridge CB30FS, UK

Virendra Parab, Prof. Sanjiv Sambandan
Department of Instrumentation and Applied Physics, Indian Institute of Science, Bangalore,
560012, India
E-mail: sanjiv@iisc.ac.in

Abstract

Thin film transistor circuits on flexible substrates is the big promise for next generation human-machine interface systems. However, a major bottleneck is the reliability of the interconnect that is prone to open circuit faults due to mechanical, electrical and environmental stress. Here we demonstrate self-healing interconnects in thin film transistor circuits on flexible substrates resulting in the restoration of > 99% of the pre-fault current. The active material for self-healing is a dispersion of conductive particles in an insulating fluid that is contained over the interconnect. Healing is triggered by the electric field that appears in the open gap during the occurrence of the fault. We discuss the engineering of the active material, demonstrate and analyze self-healing circuits and discuss methods to package and integrate the self-healing feature with the process flow. This work sets a new benchmark for reliable inkjet-printed thin film transistor circuits on flexible substrates.

1. Introduction

Inkjet-printed thin film transistor (TFTs) promise tailor-made circuits on mechanically rigid and flexible substrates for applications such as flexible displays, large area sensors and wearable electronics.[1]-[7] In such applications, the circuit experiences mechanical stress from repeated bending and stretching, thermal strain, electrical stress caused by electrostatic discharge (e.g. from human contact) or electromigration and environmental corrosion due to moisture (e.g. sweat) [8]-[14]. Thus, the reliability of the interconnect becomes important as open circuit failures become more probable. [10]-[13]

There have been three strategies adopted to tackle the problem of open circuit faults. The first has been the development of conductive materials with low elastic modulus permitting stretchable interconnects.[15]-[18] The second has been the design of interconnects using geometries that lowers its stiffness. [19]-[22] While both these approaches improve the robustness of the interconnect to mechanical stress, they do not offer any recovery if a fault were to occur due to other causes e.g. electrical stress. The third strategy has been the development of technologies that permit real-time repair (self-healing) of open circuit faults. [23]-[40]

Self-healing interconnects have been demonstrated using several methods. One has been the use of liquid metals encapsulated over the interconnect such that upon the fracture of the interconnect, the liquid metal flows into the open gap to restore conductivity. Various methods of packaging the liquid metal such as microfluidic channels, [23], [24] encapsulation in fragile insulating shells, [25]-[27] encapsulation in elastomeric substrates have been demonstrated.[28] Other techniques have used self-restructuring conductive polymers, [29], [30] hydrophobicity driven healing, [31] magnetic field induced healing and impedance modulation via the use of an external control system. [32], [33] While all these approaches are effective, they have certain

shortcomings as they either use an external controller or use relatively rare materials (eg. Ga, In), alter conventional interconnect fabrication processes, or only repair faults occurring due to mechanical stress.

Yet another self-healing technique that avoids the above shortcomings and that is of interest to this work is the electric field assisted healing using dispersions of conductive particles in insulating fluids. [34]-[40] The electric field appearing in the open gap during the occurrence of an open circuit fault initiates self-healing and results in the particles of the dispersion chaining up to form a conductive bridge across the gap thereby re-establishing electrical connectivity. This technique has several advantages. First, it permits self-healing in a current carrying interconnect irrespective of the cause of failure. Second, the technique permits stretchable interconnects with the stretching possible by an increase in the number of particles.[39] Third, since the technique uses weak dispersions, it avoids stringent packaging requirements needed to discourage accidental short-circuits.[40]

While all the above studies have benchmarked exciting progress towards realizing self-healing interconnects, none of them have been used to self-heal open circuit faults in printed TFT circuits. In this work we demonstrate the self-healing of open circuit faults in ink-jet printed organic TFT circuits on flexible substrates using electric field assisted healing.

2. Results and Discussions

2.1. Mechanism of Self-Healing

To understand the mechanism of electric field assisted self-healing we consider the case of an open circuits fault occurring in a current carrying interconnect (**Figure 1**). The active material

that enables self-healing is an inherently insulating dispersion of metallic micro-particles in an insulating fluid that is contained and isolated over the interconnect.

Upon the occurrence of an open fault in the interconnect, an electric field of magnitude, ξ, appears in the open gap. The conductive particles of the dispersion present in the open gap are now polarized to have a dipole moment, P, that scales as $P \sim r_p^3 \epsilon_f \xi$. Here r_p is the radius of the particles and ϵ_f the permittivity of the insulating fluid with $\sim$ representing a scaling relation. The polarized particles now experience dipole-dipole attractive forces of magnitude, F_p, that scales as $F_p \sim P^2 / \epsilon_f x^4$ with x being the distance between the particles. This attractive force is opposed by the viscous drag experienced by the particles moving through the insulating fluid. With time, the particles in the open gap chain up to form multiple bridges across the gap thereby weakly repairing the fault. If the length of the open gap is s, the time taken to form these bridges, τ_h, can be shown to scale as $\tau_h \sim (\eta_f / \epsilon_f)(s x^5 / r_p^6)(1/\xi^2)$ with η_f being the viscosity of the fluid.

These resistive bridges composed of electrostatically held particles establish a small current through the interconnect. This current causes Joule heating leading to a weak sintering of the particles in one of the bridges, typically the one having the shortest length. Due to the low thermal mass of the bridge and the poor thermal conductivity of the fluid, this process occurs very rapidly. Sintering reduces the resistance of the bridge significantly resulting in a rapid restoration of current through the interconnect. The broken interconnect is said to be 'healed' at this point with the sintered bridge being the 'heal' (see **Movie S1** and **Movie S2**). Upon the completion of healing, the electric field in the gap vanishes due to the low resistance of the heal. With the absence of a strong field, not only does the formation of bridges stop, but the existing bridges of electrostatically held particles dissipates as well.
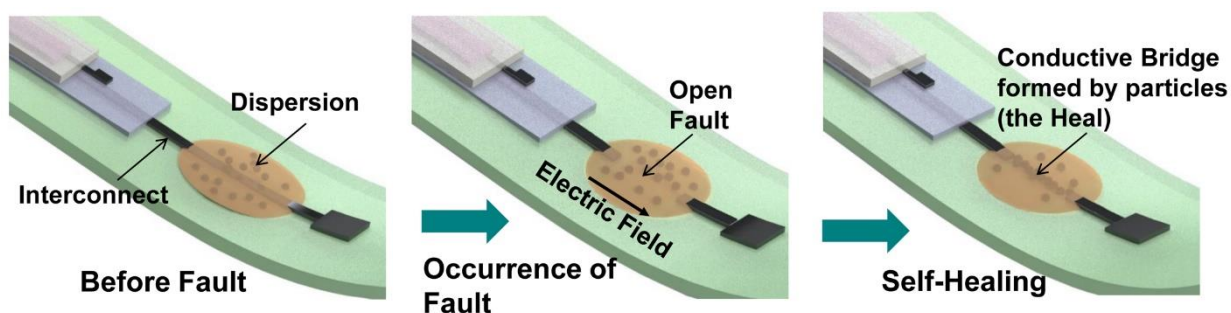
Figure 1. Mechanism of electric field assisted self-healing. The active material is a dispersion of conductive particles in an insulating fluid that is printed or dispensed over the interconnect. The occurrence of a fault in a current carrying interconnect results in an electric field in the open gap. This field polarizes the particles resulting in them experiencing dipole-dipole attractive forces resulting in them chaining up to form a heal. The formation of the heal destroys the field and stops the process.

2.2. Engineering the Dispersion for Self-Healing Thin Film Transistor Circuits

The challenges in achieving self-healing of open faults in printed circuits are a consequence of a simple but important requirement that the dispersion be inherently insulating while at the same time have enough particles to achieve self-healing. This feature reduces cross-talk between adjacent interconnects and relaxes the requirement on packaging by preventing accidental short circuits between different interconnects thereby improving reliability and easing manufacturability.

The consequence of this requirement is that the size of the conductive particles in the dispersion, defined by the particle radius r_p, be much smaller (at least about 10 times smaller) than the minimum feature size permitted by ink-jet printing. With the typical printed feature sizes being of the order of 10 μm, the dispersion must consist of conductive particles of $r_p \sim 1$ μm or less.

This results in a cascade of limitations that begins with the magnitude of the driving force for self-healing defined by the dipole-dipole attractive force, F_p, between the electrically polarized conductive particles lying in the open gap of the fault. Since $F_p \propto P^2$ and since $P \propto r_p^3$, the driving force $F_p \propto r_p^6$. Therefore, reducing r_p may reduce F_p to below that required to overcome friction and increase the relative importance of Brownian motion. This could result in a loss of self-healing ability. Even if the particles do manage to overcome friction and begin aggregating, the time taken to heal, $\tau_h \propto 1/r_p^6$, would be significantly large.

Nevertheless, since a small r_p is a requirement, we need to look to other means to improve F_p and reduce τ_h. There exist two viable options. First, since $F_p \propto \xi^2$, the electric field ξ could be increased by increasing the supply voltage. However, this is constrained by the maximum operating voltage of the TFT. Second, since $F_p \propto 1/x^4$, the inter particle distance x can be reduced by increasing the concentration of the particles in the dispersion. This is viable but needs to be done with caution to ensure that the concentration stays well below the percolation limit so as to ensure an inherently insulating dispersion.

We found that for 1 μm Ag particles dispersed in silicone oil, this optimum dispersion concentration is found to lie between 10 mg/ml to 20 mg/ml (see **text S1** in Supplementary Material). As silicone oil is non-ionic, a stearic stabilizing ligand (oleic acid) having affinity towards the silicone oil was chosen to stabilize the dispersion.[40] Oleic acid treated 1 μm Ag particles were found to de-flocculate sufficiently resulting in a stable and homogenous dispersion (see **Figure S1**, and **Figure S2** in Supplementary Material).

2.3. Characterizing Self-Healing in Inkjet Printed Interconnects

Self-healing in ink-jet printed interconnects on polyethylene naphthalate (PEN) substrate was characterized using the experimental setup shown in **Figure 2a**. Open faults of widths $s\sim20$ μm and $s\sim80$ μm were purposely introduced in the interconnect. The interconnect was connected to a source-measure-unit (SMU) via an external resistor of resistance, R_{ext}. The dispersion of 1 μm Ag particles in silicone oil was dispensed over the open fault. The SMU was then used to apply a dc voltage, V_{ext}, and monitor the dynamics of the current through the interconnect. The magnitude of the maximum current and the time taken for healing, τ_h, were extracted from the dynamics of current. **Figure 2b** illustrate the sequence of images during healing (also see supplementary **Movie S2**). The figure also shows helium ion microscopy images of the sintered heal.

Figure 2c shows the impact of varying the dispersion concentration. The heal time, τ_h, was obtained from the dynamics of the current during healing for three different concentrations i.e. 10 mg/ml, 20mg/ml and 40 mg/ml. The distribution of τ_h across several experiments with $s\sim80$ μm gap is also shown. The dashed line shows the trend of the mean τ_h versus dispersion concentration on a log-log scale. It is seen that τ_h varies as the -3/2 th power of the concentration. For 10 mg/ml and 20 mg/ml, the dispersion was inherently insulating (see **Figure S3** in Supplementary Material) and healing was observed with $\tau_h\sim10$ s-100 s and $\tau_h\sim1$ s-10 s, respectively. In the case of 40 mg/ml dispersions, many samples were inherently conductive while some non-conductive samples showed much quicker healing with $\tau_h\sim0.01$ s-1 s. However, this high concentration is undesirable as it is preferable to have inherently insulating dispersions to improve reliability during packaging. In conclusion, the optimum dispersion concentration for 1 μm Ag particles in silicone oil is about 20 mg/ml and this agrees with calculations (see supplementary material **text S1**).
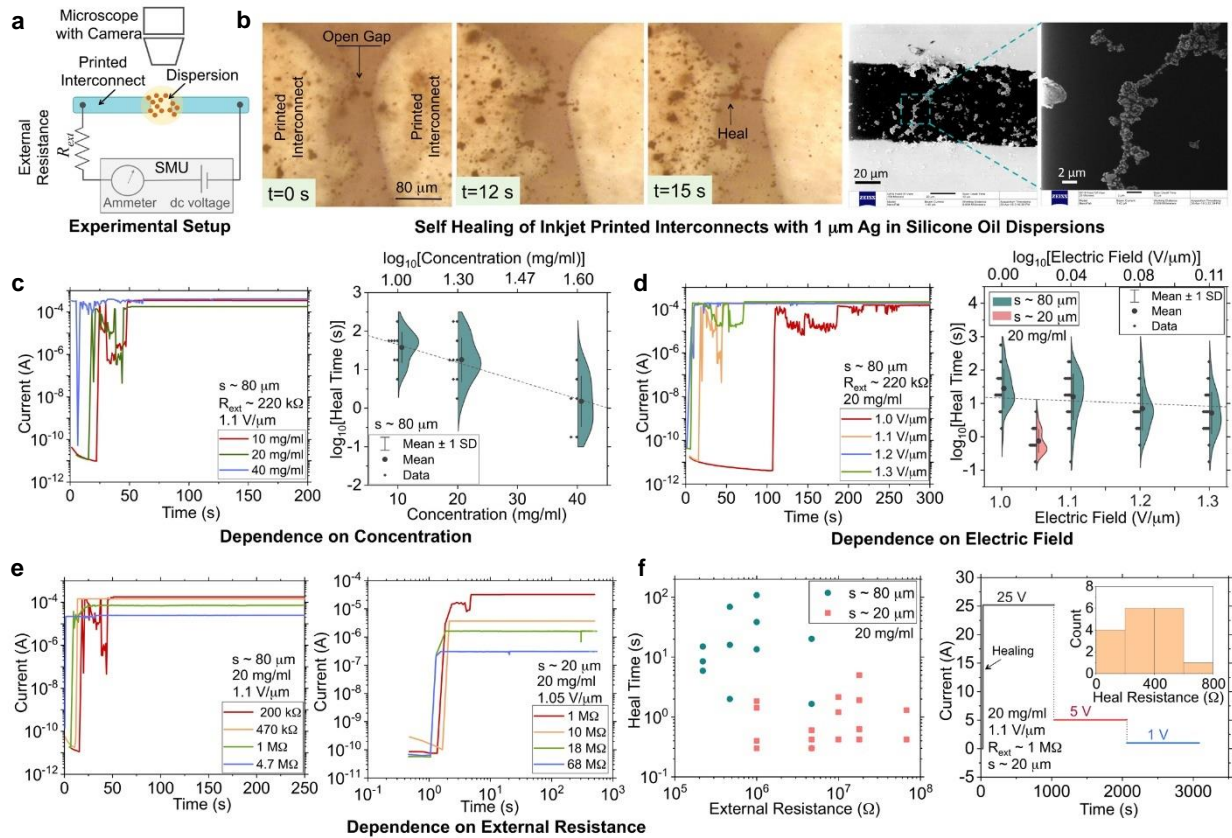
Figure 2. Self-healing of ink-jet printed interconnects on flexible substrates. (a) Schematic of experimental setup used for studying the dynamics of self-healing. (b) Snapshots capturing stages healing (also see Movie S2) and helium ion micrographs of the sintered heal. (c) Typical dynamics of current for dispersion concentration of 10 mg/mL, 20 mg/mL and 40 mg/mL and the dependence of heal time on dispersion concentration. (d) Typical dynamics of current for different electric field strengths of 1.0 V/µm, 1.1 V/µm, 1.2 V/µm and 1.3 V/µm and the dependence of heal time on the field strength for fault size of 80 µm and 20 µm. (e) (Left) Dynamics of heal current for different external resistances for 80 µm and 20 µm open gaps. (f) Distribution of heal time against external resistance and the stability of the heal when the external voltage is sequentially lower. The typical heal impedance is about 500 Ω.

Figure 2d shows the impact of electric field, ξ, on heal time. Experiments were performed using 20 mg/ml dispersions with open gap length $s{\sim}80$ µm. For each sample, the electric field was set at a specific value by first measuring the length of the open gap, s, and subsequently applying the appropriate voltage to the circuit. Healing was not consistent for $\xi < 0.6$ V/µm. For $\xi > 1.3$ V/µm healing occurred rapidly but the heal was unable to sustain the large current

resulting in open faults once again. The optimum zone for consistent healing was 0.6 V/μm ≤ ξ < 1.3 V/μm and **Figure 2d** shows the distribution of τ_h as a function of ξ lying in this range. The dashed line shows the trend of the mean τ_h versus ξ on a log-log scale. It is seen that τ_h varies as $1/\xi^2$ as predicted by theory. The case of healing an open gap length of $s \sim 20$ μm with $\xi \sim 1.05$ V/μm is of interest with regards to TFT circuits since this corresponds to the typical operating voltage for TFTs.

Figure 2e shows the impact of the external resistance, R_{ext}, on the heal time. As the initial field across the gap $\xi \sim V_{ext}/s$ is independent of R_{ext}, the time taken for healing does not show any consistent trend with R_{ext}. However, R_{ext} would determine the dynamics of sintering. It was found that large open gaps (here $s \sim 80$ μm) did not show successful healing at large R_{ext} (for $R_{ext} > 4.7$ MΩ). On the other hand, successful healing was observed for smaller open gaps ($s \sim 20$ μm) even for large R_{ext} (upto $R_{ext} \sim 68$ MΩ). This is significant from the point of view of self-healing of TFT circuits.

The impedance of the TFT is to first order given by $\left[\mu C_i (W/L)\left(V_{gs} - V_T\right)\right]^{-1}$. For organic p-type TFTs with mobility μ =0.1 cm²/Vs, dielectric capacitance per unit area C_i =10 nF/cm², channel width, W =1000 μm, channel length L =100 μm, threshold voltage $V_T = -1\,V$ and gate-source voltage V_{gs} =-11 V, the resistance offered by the TFT is 10 MΩ. The results of Fig. 2e imply that self-healing of organic TFT circuits would likely be possible if the open gap is $s \sim 20$ μm.

Figure 2f shows the stability of the heal. In this experiment, an open circuit fault with $s \sim 20$ μm was purposely created in the printed interconnect with $R_{ext} = 1$ MΩ. Healing was then achieved by applying an external voltage V_{ext} =25 V applied for 1000 s. The voltage was then

reduced to $V_{ext} =5$ V for 1000 s and subsequently $V_{ext} =1$ V for 1000 s and in both these cases, the electric field was expected to be < 0.5 V/mm. The current through the interconnect was continuously monitored through the experiment. After healing, the current was observed to be stable and dependent on R_{ext} alone, indicating the permanence and low resistance of the heal. A histogram of the steady state heal resistance is shown in the inset. The typical heal resistance in steady state is ~ 500 Ω.

2.4. Self-Healing in Inkjet-Printed TFTs

Self-healing in ink-jet printed TFTs on PEN substrate was characterized using bottom-gate, bottom-contact TFTs with a 80 nm thick Ag gate, 480 nm thick polyvinyl cinnamate (PVCN) dielectric (see Supplementary Material, **Figure S4**), 80 nm thick Ag source and drain and 6,13 bis(triisopropylsilylethynyl) pentacene (TIPS-pentacene) semiconductor (see Methods). **Figure 3a** shows a micrograph of the printed TFT along with the typical transfer and output characteristics. The devices exhibited a field effect mobility of ~ 0.166 cm^2/Vs, threshold voltage of $\sim$-2 V, on–off switching ratio of $\sim 10^6$ and showed no hysteresis.

Self-healing in TFT circuits was characterized using the experimental setup shown in **Figure 3b**. The setup is like that of **Figure 2** but with the external resistance being replaced by the p-type TFT having channel width 1600 μm and channel length 80 μm. The source of the TFT was kept at ground, the drain and gate were provided dc bias voltages, $V_d < 0$ and $V_g < 0$ with respect to ground, respectively.
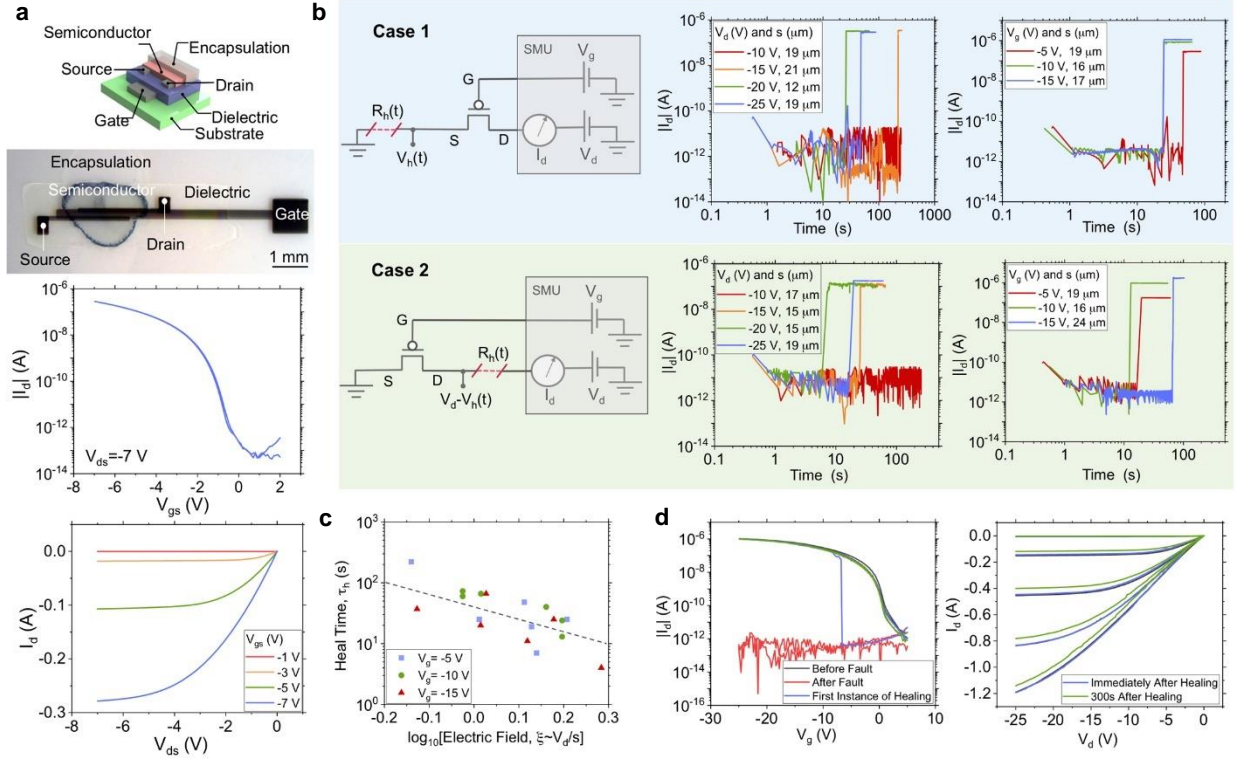
Figure 3. Self-healing of interconnects for ink-jet printed organic TFTs. (a) Schematic and micrograph of a printed TFT along with the typical transfer and output characteristics. (b) Evaluation of dynamics of transistor drain current during self-healing. Case 1 – the fault located at the source, Case 2- the fault located at the drain. (c) Impact of heal time on the drain-source voltage (d) The transfer and output characteristics of the organic TFT before and after healing.

Two experiments were performed - Case 1 and Case 2, as shown in **Figure 3b**. In Case 1, an open fault of length s was purposely created in the interconnect between the ground probe and source. In Case 2, an open fault of length s was purposely created in the interconnect between V_d and drain. Both experiments were started by dispensing the dispersion over the fault and applying voltage bias at the three pads, i.e. ground, $V_d \leq 0$ and $V_g - V_T \leq 0$, while monitoring the dynamics of the current through the TFT. In both experiments, the time varying heal resistance caused a time dependent voltage drop, $V_h(t)$, across the heal. However, the key difference between the two experiments is that in Case 1, the voltage drop across the heal, $V_h(t)$, affected both the gate-source voltage as well as the drain-source voltage of the TFT whereas in Case 2, $V_h(t)$ affected only the drain-source voltage and not the gate-source voltage.

11

In Case 1, at time $t = 0$, the large resistance of the open fault caused $V_h(t = 0) \sim V_d < 0$ resulting in an electric field V_d/s in the open gap. The gate-source overdrive voltage was $V_g - V_h(t) - V_T \approx V_g - V_d - V_T$. The process of healing increased $V_h(t)$ from $V_h(t = 0) \sim V_d < 0$ to $V_h \sim 0$ thereby making $V_g - V_h(t) - V_T \approx V_g - V_T$ and turning on the TFT. However, the exact dynamics depended on whether $V_g - V_d - V_T < 0$ or whether $V_g - V_d - V_T \geq 0$. If $V_g - V_d - V_T < 0$, the TFT was initially on (channel formed) and biased in deep linear operation with zero drain-source voltage. After healing, the TFT continued to operate in linear operation. If on the other hand, $V_g - V_d - V_T \geq 0$, the TFT was initially off or in subthreshold operation. Yet, due to the presence of the field in the gap, healing occurred despite the large TFT resistance. After healing, the TFT turns on and is biased in saturation mode operation.

In Case 2, at time $t = 0$, $V_h(t = 0) \sim V_d < 0$ resulting in an electric field V_d/s across the open gap with the drain-source voltage of the TFT being zero. The gate-source overdrive voltage of the TFT remains unaffected and equal to $V_g - V_T < 0$. Therefore, in this case, irrespective of the value of V_d, the TFT was always turned on. At time $t = 0$, the TFT was in deep linear bias. After healing the TFT operated in linear mode if $V_g - V_d - V_T < 0$ or in saturation mode if $V_g - V_d - V_T \geq 0$.

Figure 3b shows the dynamics of current during self-healing and the impact of the TFT bias for both cases. The length of the open gap, s, was measured for each experiment and is defined in the legend. In both cases, it was observed that the electric field in the gap was a dominant parameter that decided the time taken for self-healing. Healing was not observed for $V_d/s < 0.7$ V/µm. Healing within 200 s was consistently observed for $V_d/s > 0.7$ V/µm. This is in corroboration with the conclusions of **Figure 2**. This also poses a limit on the bias or length of

the open gap for which healing is possible. For example, if the maximum operating voltage of the TFT of 30 V, successful self-healing would be possible for $s \leq 42$ μm. **Figure 3c** summarizes the impact of the electric field on the heal time for different gate voltages. The dashed line has a slope of -2 and corroborates the $1/\xi^2$ dependence of the heal time on electric field.

Figure 3d compares the transfer and output characteristics of the TFT before fault and after heal. The transfer characteristics of the pristine TFT (before fault) was first measured by setting V_d = -25 V and sweeping V_g from +5 V to -25 V and then back to +5 V to check for hysteresis. The output characteristics of the TFT was then subsequently measured. Then, an open circuit fault ($s \sim 20$ μm) was purposely created in the interconnect joining the ground probe and the source of the TFT. The transfer characteristics of the TFT (after fault) was measured once more indicating the failure of the TFT. Subsequently, the dispersion was dispensed over the region of the fault and V_g was repeatedly swept till healing occurred. The fault was consistently found to heal during the first sweep after the dispensing of the dispersion. The completion of healing was seen by the abrupt rise of current from 'after fault' levels to 'before fault' levels. After the first instance of healing, the output characteristics of the TFT was measured. Finally, the transfer and output characteristics were again measured 300 s after the first instance of healing to check for stability. The heal was found to be stable.

2.5. Self-Healing in Inkjet-Printed Voltage Amplifiers

To study the impact of self-healing on TFT circuits, inkjet-printed p-type TFT based single stage voltage amplifiers were fabricated on PEN substrates (**Figure 4a**). Experiments on self-healing were performed using the amplifier in common source configuration. Since both driver and load were p-type TFTs, the theoretical magnitude of the small signal gain was expected to

be the ratio of the transconductance of the driver TFT to the load TFT. For this particular study, the load and driver TFTs were designed to be geometrically identical with channel width of 1600 μm and channel length of 80 μm predicting a voltage gain of -1. Any other value of gain is attributed to mismatch in device parameters. The amplifier was driven with a dc supply voltage V_{DD} =30 V. The input voltage, V_{in}, was supplied to the driver TFT while the load was diode connected to ground.

To demonstrate healing, open circuit faults ($s \sim 20$ μm) were purposely introduced in the amplifier as shown in **Figure 4b**. Three cases were studied based on the location of the fault – Case 1, Case 2 and Case 3. In Case 1, the fault was in the interconnect joining the source of the driver TFT and V_{DD}. In this case any heal resistance would act as a degeneration resistor to the common source amplifier. In Case 2, the fault was located between the drain of the driver TFT and the output node. In Case 3, the fault was located between the drain of the load TFT and ground.

During experiments, the amplifier transfer characteristic for each case was measured before the creation of the fault by sweeping V_{in} from +5 V to -35 V with the corresponding output voltage V_{out} measured (**Figure 4b**). The characteristic was then measured after the creation of the fault. Subsequently, the dispersion was dispensed over the region of the fault and the transfer characteristic was periodically measured till healing occurred. The fault was consistently found to heal during the first sweep after the dispensing of the dispersion. The completion of healing was seen by the abrupt change in V_{out} from 'after fault' levels to 'before fault' levels. After the first instance of healing, the transfer characteristics of the TFT was measured again after 300 s. The heal was found to be stable.
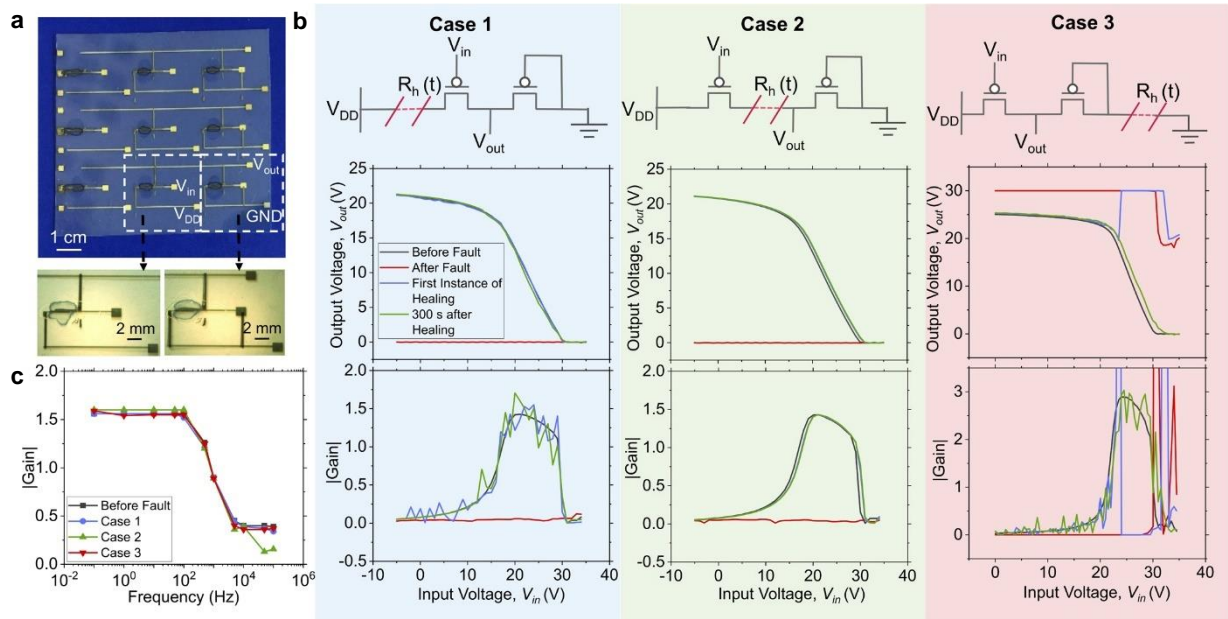
Figure 4. Self-healing of interconnects for organic TFT-based common-source amplifier. (a) Micrographs of common source amplifiers on PEN substrate. Enlarged photographs showing the load and driver TFTs. (b) Self-healing in single stage voltage amplifier circuit with the fault located at various locations as defined by three cases. (c) Frequency response of the amplifier before fault and after healing for each of the cases.

The frequency response of the amplifier was also measured for all cases. The Bode magnitude plot is shown in **Figure 4c**. There was no significant change in the frequency performance measured after healing compared to that measured before the creation of the fault. The amplifier showed a - 3dB cut-off frequency at around 500 Hz before and after healing, irrespective of the location of the fault.

2.6. Integration and Packaging

All the above studies on self-healing were performed by dispensing the dispersion over the known location of the open fault. However, to achieve manufacturability, the dispersion needs to be encapsulated or contained along the interconnects without interfering with circuit operation.

There are two approaches to achieve this. The first approach is to borrow ideas from microfluidic techniques and contain the dispersion in microchannels built into soft materials (eg. polydimethylsiloxane) and located along the interconnects. While feasible, this approach requires a significant increase in manufacturing complexity when it comes to high density circuits. The second approach is to take advantage of the inherently insulating nature of the dispersion and dispense the dispersion all over the substrate without any containment. The TFTs could be encapsulated and a simple design rule that limits the maximum electric field between different interconnects would avoid unwanted short circuits. While easier to implement, this approach tends to increase the possibility of accidental short circuits.

Using a combination of both concepts, an approach as described in **Figure 5a** was tested. The PEN substrate was patterned into oleophilic and oleophobic regions by coating Trichloro(1H,1H,2H,2H-perfluorooctyl) silane (97%, Sigma Aldrich) by evaporation and by use of a shadow mask. The interconnects and devices were then printed in the oleophilic regions while the oleophobic regions separated different interconnects. The dispersion was then dispensed freely over the substrate and remained confined in the oleophilic regions. **Figure 5a** shows the cross-section image of the confined dispersion. Also shown is the comparison of the spread of the dispersion with and without oleophobic treatment. **Figure 5a** also shows the performance of the TFT printed on the treated substrate before fault, after fault and after healing. The performance of the TFT and the ability of self-heal remained unaffected by oleophobic treatment. While further studies are needed, this approach showed promise with regards to scaling up and manufacturing flexible electronic platforms with the self-healing ability integrated with TFT circuits.
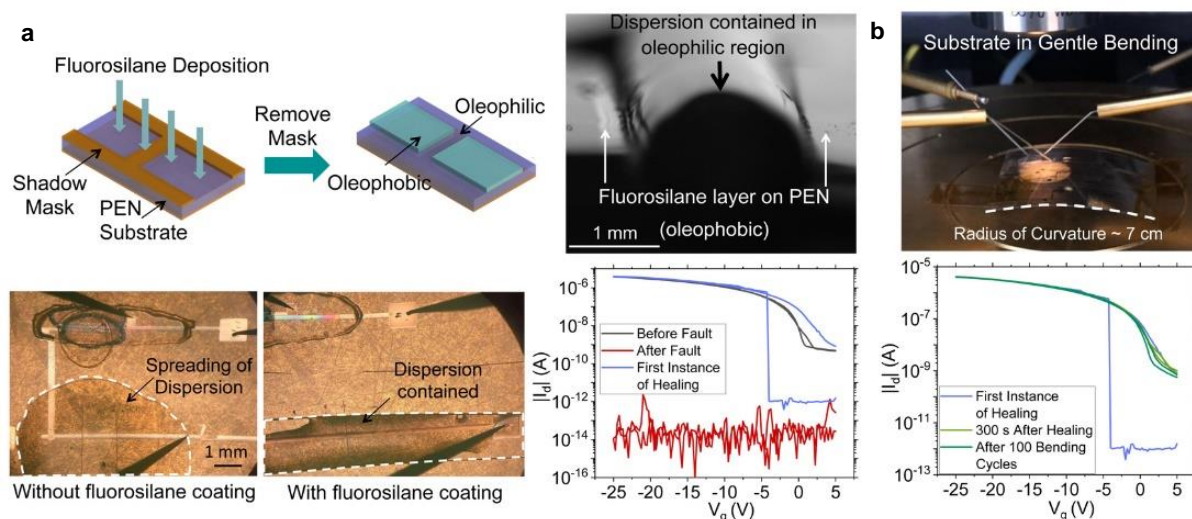
Figure 5. (a) Method to package the dispersion using an ink-jet printing compatible process and add self-healing ability to a circuit. The dispersion is prevented from leaving the containment zone by patterning the substrate into oleophobic regions (by silane treatment). Also shown is the cross section image demonstrating containment of the suspension between silane treated regions. Also shown is the successful self-healing achieved with the above described packaging. (b) Self-healing with bending (bending radius ~ 7 cm) and demonstration of heal stability after 100 bending cycles.

2.6. Impact of Bending

The impact of gentle bending on the heal is shown in **Figure 5b**. An open fault was purposely created in the interconnect between the source of the TFT and ground. The substrate was then gently bent to have a radius of curvature of ~7 cm. Contacts were drawn out and the bent substrate was connected to the SMU. The dispersion was then dispensed over the open gap. The transfer characteristics of the TFT was then measured periodically till healing occurred. After the first instance of healing, the substrate was removed and subjected to repeated bending for 100 cycles. The TFT characteristics was measured once again. **Figure 5b** shows the transfer characteristics of the self-healed TFT circuit remained unaffected by bending.

3. Conclusion

To summarize, electric field assisted self-healing of inkjet printed TFT based circuits on PEN substrates was demonstrated. The optimum dispersion was engineered to be 20 mg/ml of 1 μm Ag particles in silicone oil. Oleic acid functionalization achieved reasonably good stabilization. This dispersion was inherently insulating and yet allowed for rapid self-healing. Experiments showed self-healing in ink-jet printed interconnects to be most effective when the fault resulted in an electric field that was > 0.7 V/μm but < 1.3 V/μm. Therefore, effective healing of open faults of about 20 μm lengths were easily healed when the voltage across it was > 14 V and when any external impedance was < 70 MΩ. Moreover, stable healing with the heal having an impedance of 400 Ω was consistently achieved. Thus, the engineered dispersion was ideal for TFT circuits. Subsequently TFT circuits were shown to heal when the fault was located at any point in a current carrying path. Due to the low heal impedance of 400 Ω, the dc output and transfer characteristics of TFTs and ac characteristics of TFT based amplifiers post-heal were identical to pre-fault conditions with no observed hysteresis. The heal was also shown to be stable under repeated gentle bending of about 7 cm radius of curvature. Multiple simultaneous faults was also shown to be healed. The electronic noise due to the heal was shown to be negligible. Most importantly, a method of using oleophobic surfaces to contain the dispersion over the interconnects and thereby package the dispersion onto the substrate having printed circuits was demonstrated. This allows for the self-healing feature to be made available as an add-on feature for printed electronics. These results increase the possibility of having thin film transistor circuits on flexible substrates with an ability to heal themselves.

Materials and Methods

Chemicals

Silver (Ag) ink (JET 605C) for inkjet printing was purchased from Hisense Electronics, Kunshan, China. Silicone oil (viscosity 350 cSt @ 25 °C), Anisole, polyvinyl cinnamate (PVCN), 6,13 bis(triisopropylsilylethynyl) pentacene (TIPS-pentacene), polystyrene (PS), perfluorobenzenethiol (PFBT) were purchased from Sigma Aldrich. CYTOP^{TM} (CTL-809M) and its thinner (CT-Solv. 180) were purchased from Asahi Glass, Japan. Silver powder, APS 0.7-1.3 micron, 99.9% (metals basis) was purchased from Alfa Aesar. Oleic acid (> 70%) and ethanol (99%), extra pure, SLR grade was purchased from Fischer Scientific. Polyethylene naphthalate (PEN) substrates (Teonex Q65HA, 125 µm) were purchased from Pütz GmbH & Co. Folien KG. All chemicals were used without any purification.

Fabrication and characterization of TFT circuits

Inkjet printing of TFTs on PEN substrate was carried out with DMP-2831 material inkjet printer (Fujifilm, Dimatix). The structure of the fully-printed bottom-gate bottom-contact organic TFT consisted of Ag for Gate electrode, PVCN for dielectric layer, followed by another Ag film for source/drain electrodes, TIPS-pentacene blended with PS for semiconductor layer, and CYTOP^{TM} for passivation layer.

The ink preparation for each layer is detailed below. The PVCN was dissolved in anisole with a concentration of 45 mg/ml. The semiconductor ink was prepared by blending the respective solution (10 mg/mL) of TIPS-pentacene and PS in anisole with a volume-to-volume ratio of 3:1. All inks were stirred by a magnetic stirrer and injected into a cartridge (DMPLCP-11610, Dimatix) through a 0.2 µm PTFE (Teflon) filter. The typical sheet resistance of the Ag films was 25 Ω/sq to 30 Ω/sq.

The gate electrode was printed using Ag ink with a 50 μm drop spacing, annealing at 130 ℃ for 15 min, to form the conductive film. [42] Then PVCN film was deposited as two print layers with a drop spacing of 10 μm, followed by a 30 min exposure to UV light (254 nm) in curing equipment for cross-linking and 30 min annealing at 100 ℃. The source and drain electrodes were printed like gate electrode and annealed at 120 ℃ for 15 min. Before the deposition of the semiconductor layer, source-drain electrodes were treated by a PFBT-ethanol solution (PFBT:ethanol = 1:1000) for 15 min and rinsed with pure ethanol, followed by a 1-minute annealing. Then the TIPS-PS blended solution was deposited with a drop spacing of 10 μm, annealed at 100 ℃ for 10 min. Finally the CYTOP^{TM} (CYTOP:thinner = 1:3) was dropped on the channel area as the encapsulation, preventing the oxygen and water from the semiconductor.[43] The transfer and output characteristics of the devices were measured by Keithley 4200-SCS.

Oleic acid treatment of silver powder

A 10 mg/mL suspension of silver powder in oleic acid was stirred vigorously at 35 °C for 24 hrs. The suspension was then centrifuged at 4500 RPM for 20 min to remove the supernatant. The silver powder was resuspended in ethanol then centrifuged to remove the excess oleic acid. After three successive washing cycles in ethanol, the silver particles are dried overnight. The desired amount of OA (oleic acid) coated silver powder was added to silicone oil and mixed with a vortex mixer for 1 min. The dispersion was then sonicated in a water bath for 5 min before its use for self-healing.

Heal dynamics video recording

The video recording of the heal dynamics was captured with Olympus DP-71 with 20X lens with frame rate of 30 fps.

Helium-Ion microscope recordings

The sample for healed bridges across inkjet printed electrodes were wiped for the residue of healing suspension around the electrode gap. A few drops of isopropyl alcohol (LR Grade, 99%) were rolled across the gap to remove residual oil and dried in ambiance. The sample was then subjected to oxygen plasma for 90s, with Diener-electronic Femto plasma system. The bridge was imaged in ZEISS NanoFab He ion microscope. The imaging voltage was 20 kV.

Surface treatment of PEN for integration and packaging

PEN substrate was coated with oleophobic film to contain the healing dispersion on selective area. The selective coating was achieved by vacuum deposition of Trichloro(1H,1H,2H,2H-perfluorooctyl)silane (97%, Sigma Aldrich) on PEN substrate with shadow mask.

Supporting Information

Supporting Information is available from the Wiley Online Library or from the author.

Author Contributions

L.D fabricated printed interconnects, printed TFTs and printed TFT circuits and performed all measurements regarding self-healing with TFT circuits, P. J prepared the dispersion for self-healing experiments and performed all measurements regarding self-healing with inkjet printed interconnects, P. J. performed surface treatment of the substrate for packaging and integration

of self-healing with thin film transistor circuits, P.J and L.D tested the self-healing of packaged TFTs. J.M. acquired the contact angle measurement images and videos for silane treated and untreated surfaces, S.S directed the research. All authors analyzed the results and contributed to the paper.

References

[1]   F. Molina-Lopez, T. Z. Gao, U. Kraft, C. Zhu, T. Öhlund, R. Pfattner, V. R. Feig, Y. Kim, S. Wang, Y. Yun, Z. Bao, Inkjet-printed stretchable and low voltage synaptic transistor array. *Nat. Commun.* **2019**, *10*, 2676.

[2]   M. Gao, L. Li, Y. Song, Inkjet printing wearable electronic devices. *J. Mater. Chem. C.* **2017**, *5*, 2971–2993.

[3] T. Sekitani, T. Yokota, K. Kuribara, M. Kaltenbrunner, T. Fukushima, Y. Inoue, M. Sekino, T. Isoyama, Y. Abe, H. Onodera and T. Someya, Ultraflexible organic amplifier with biocompatible gel electrodes. *Nat Commun*. **2016,** *7*, 11425

[4]   J. Liang, K. Tong, Q. Pei, A water-based silver-nanowire screen-print ink for the fabrication of stretchable conductors and wearable thin-film transistors. *Adv. Mater.* **2016**, *28,* 5986–5996.

[5]   P. M. Grubb, H. Subbaraman, S. Park, D. Akinwande, R. T. Chen, Inkjet printing of high performance transistors with micron order chemically set gaps. *Sci. Rep.* **2017**, *7*, 1202.

[6]   S. Chung, K. Cho, T. Lee, Recent progress in inkjet-printed thin-film Transistors. *Adv. Sci.* **2019**, *6,* 1801445.

[7]   D. H. Kim, N. Lu, R. Ma, Y. S. Kim, R. H. Kim, S. Wang, J. Wu, S. M. Won, H. Tao, A. Islam, K. J. Yu, T. Il Kim, R. Chowdhury, M. Ying, L. Xu, M. Li, H. J. Chung, H. Keum, M. McCormick, P. Liu, Y. W. Zhang, F. G. Omenetto, Y. Huang, T. Coleman, J. A. Rogers, Epidermal electronics. *Science.* **2011,** *333*, 838–843.

[8] P. Bhattacharya, R. Sinha, B. Thakur, V. Parab, M. Shrivastava, S. Sambandan, Adaptive Dielectric Thin Film Transistors - A Self-Con guring Device for Low Power Electrostatic Discharge Protection, IEEE Electron Device Letts. 2019, 41, 66-69.

[9] W. Zeng , L. Shu , Q. Li , S. Chen , F. Wang, X.-M. Tao, Fiber-Based Wearable Electronics: A Review of Materials, Fabrication, Devices, and Applications, *Adv. Mater.* **2014,** *26*, 5310-5336. https://doi.org/10.1002/adma.201400633

[10] E. Sowade, E. Ramon, K. Y. Mitra, C. Martínez-Domingo, M. Pedró, J. Pallarès, F. Loffredo, F. Villani, H. L. Gomes, L. Terés, R. R. Baumann All-inkjet-printed thin-film transistors: manufacturing process reliability by root cause analysis. *Sci Rep* **2016**, *6*, *33490* https://doi.org/10.1038/srep33490

[11] H. Gleskova, S. Wagner, and Z. Suo, a-Si:H thin film transistors after very high strain *J. of Non-Crystalline Solids* **2000**, *266-269, 1320-1324*.

[12] J. H. Seo, Corrosion Protection of Aluminum Data Line in TFT-LCD Using Chemical Conversion Coating *Solid State Phenomena*, **2007,** *124-126, 1553–1556*. https://doi.org/10.4028/www.scientific.net/ssp.124-126.1553

[13]　S. Sambandan, R. B. Apte, W. S. Wong, R. Lujan, M. Young, B. Russo, S. Ready, R. A. Street, Defect identification in large area electronic backplanes. *IEEE/OSA J. Disp. Technol.* 2009, *5*, 27–33.

[14]　S. Daniel, A. Nair, S. Sambandan, Test System for Thin Film Transistor Parameter Extraction in Active Matrix Backplanes. *IEEE J. Electron Devices Soc.* **2019**, *7*, 638–644.

[15]　S. P. Lacour, G. Courtine, J. Guck, Materials and technologies for soft implantable neuroprostheses. *Nat. Rev. Mater.* **2016**, *1*, 16063.

[16]　V. Martinez, F. Stauffer, M. O. Adagunodo, C. Forro, J. Vörös, A. Larmagnac, Stretchable Silver Nanowire-Elastomer Composite Microelectrodes with Tailored Electrical Properties. *ACS Appl. Mater. Interfaces*. **2015, 7**, 13467–13475.

[17]　F. Xu, Y. Zhu, Highly conductive and stretchable silver nanowire conductors. *Adv. Mater.* **2012**, *24*, 5117–5122.

[18]　S. Yun, X. Niu, Z. Yu, W. Hu, P. Brochu, Q. Pei, Compliant silver nanowire-polymer composite electrodes for bistable large strain actuation. *Adv. Mater.* **2012**, *24*, 1321–1327.

[19]   R. Verplancke, F. Bossuyt, D. Cuypers, J. Vanfleteren, Thin-film stretchable electronics technology based on meandering interconnections: Fabrication and mechanical performance. *J. Micromechanics Microengineering*. **2012**, *22*, 015002.

[20]   D. H. Kim, Z. Liu, Y. S. Kim, J. Wu, J. Song, H. S. Kim, Y. Huang, K. C. Hwang, Y. Zhang, J. A. Rogers, Optimized structural designs for stretchable silicon integrated circuits. *Small*. **2009**, *5*, 2841–2847.

[21]   W. Dang, V. Vinciguerra, L. Lorenzelli, R. Dahiya, Printable stretchable interconnects. *Flex. Print. Electron.* **2017**, *2*, 013003.

[22]   J. Mertens, R. W. Bowman, J. C. W. Willis, A. Robinson, D. Cotton, R. White, K. A. Seffen, J. J. Baumberg, Scalable microaccordion mesh for deformable and stretchable metallic films. *Phys. Rev. Appl.* **2015**, *4,* 044006.

[23]   E. Palleau, S. Reece, S. C. Desai, M. E. Smith, M. D. Dickey, Self-healing stretchable wires for reconfigurable circuit wiring and 3D microfluidics. *Adv. Mater.* **2013**, *25*, 1589–1592.

[24]   G. Li, X. Wu, D. W. Lee, A galinstan-based inkjet printing system for highly stretchable electronics with self-healing capability. *Lab Chip*. **2016**, *16*, 1366–1373.

[25]   B. J. Blaiszik, S. L. B. Kramer, M. E. Grady, D. A. McIlroy, J. S. Moore, N. R. Sottos, S. R. White, Autonomic restoration of electrical conductivity. *Adv. Mater.* **2012**, *24*, 398–401.

[26]   M. M. Caruso, S. R. Schelkopf, A. C. Jackson, A. M. Landry, P. V. Braun, J. S. Moore, Microcapsules containing suspensions of carbon nanotubes. *J. Mater. Chem.* **2009**, *19*, 6093–6096.

[27]   S. A. Odom, M. M. Caruso, A. D. Finke, A. M. Prokup, J. A. Ritchey, J. H. Leonard, S. R. White, N. R. Sottos, J. S. Moore, Restoration of conductivity with TTF-TCNQ charge-transfer salts. *Adv. Funct. Mater.* **2010**, *20,* 1721–1727.

[28]   E. J. Markvicka, M. D. Bartlett, X. Huang, C. Majidi, An autonomously electrically self-healing liquid metal-elastomer composite for robust soft-matter robotics and electronics. *Nat. Mater.* **2018**, *17,* 618–624.

[29]   J. Y. Oh, S. Rondeau-Gagné, Y. C. Chiu, A. Chortos, F. Lissel, G. J. N. Wang, B. C. Schroeder, T. Kurosawa, J. Lopez, T. Katsumata, J. Xu, C. Zhu, X. Gu, W. G. Bae, Y. Kim, L. Jin, J. W. Chung, J. B.-H. Tok, Z. Bao, Intrinsically stretchable and healable semiconducting polymer for organic transistors. *Nature*. **2016**, 539, 411–415.

[30]   K. A. Williams, A. J. Boydston, C. W. Bielawski, Towards electrically conductive, self-healing materials. *J. R. Soc. Interface*. **2007**, *4*, 359–362.

[31]   X. Yong, E. J. Crabb, N. M. Moellers, A. C. Balazs, Self-Healing Vesicles Deposit Lipid-Coated Janus Particles into Nanoscopic Trenches. *Langmuir*. **2013**, *29,* 16066–16074.

[32]   A. J. Bandodkar, C. S. López, A. M. V. Mohan, L. Yin, R. Kumar, J. Wang, All-printed magnetically self-healing electrochemical devices. *Sci. Adv.* **2016**, *2*, 1601465.

[33]   S. M. Bowers, K. Sengupta, K. Dasgupta, B. D. Parker, A. Hajimiri, Integrated self-healing for mm-wave power amplifiers. *IEEE Trans. Microw. Theory Tech.* **2013**, *61*, 1301–1315.

[34]   S. Sambandan, Self repair in circuits - Automating open fault repair in integrated circuits using field-induced aggregation of carbon nanotubes. *IEEE Trans. Electron Devices*. **2012**, *59*, 1773–1779.

[35]   A. Nair, K. Raghunandan, V. Yaswant, S. S. Pillai, S. Sambandan, Maze solving automatons for self-healing of open interconnects: Modular add-on for circuit boards. *Appl. Phys. Lett.* **2015**, *106*, 123103.

[36]   V. Parab, L. Ding, A. Kumar, V. Yaswant, S. Sambandan, Self-Healing Interconnects for Reliable Flexible Electronics. *ECS Trans.* **2018**, *85,* 825–831.

[37]   J. B. Fleury, D. Pires, Y. Galerne, Self-Connected 3D architecture of microwires. *Phys. Rev. Lett.* **2009**, *103,* 267801.

[38]   V. Yaswant, A. Kumar, S. Sambandan, Self healing of open circuit faults: With active re-configurability and mimicry of synaptic plasticity. *Appl. Phys. Lett.* **2016**, *109,* 024101.

[39]   A. Kumar, V. Parab, A. Handu, L. Ding, P. Joshi, C. Jiang, S. Sambandan, Self-healing

Interconnects with Nearly Plastic Stretching of Repairs. *Phys. Rev. Appl.* **2019**, *11,* 014057.

[40]   V. Parab, O. Prasad, S. Pillai, S. Sambandan, Electric Field Assisted Self-Healing of Open Circuits with Conductive Particle-Insulating Fluid Dispersions: Optimizing Dispersion Concentration. *Sci. Rep.* **2019**, *9,* 19700.

[41]   F. Yu, Y. Chen, X. Liang, J. Xu, C. Lee, Q. Liang, P. Tao, T. Deng, Dispersion stability of thermal nanofluids. *Prog. Nat. Sci. Mater. Int.* **2017,** *27,* 531–542.
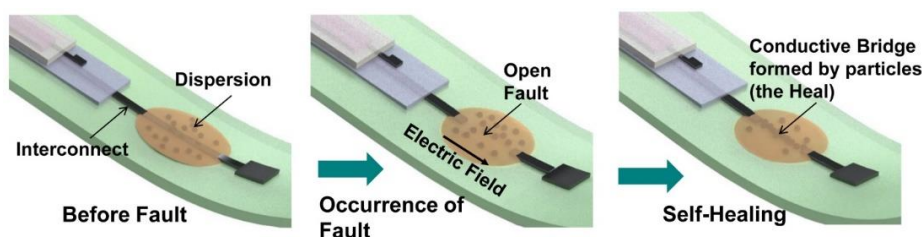
[42]   W. Tang, L. Feng, J. Zhao, Q. Cui, S. Chen, X. Guo, Inkjet printed fine silver electrodes for all-solution-processed low-voltage organic thin film transistors. *J. Mater. Chem. C.* **2014**, *2,* 1995–2000.

[43]   L. Feng, C. Jiang, H. Ma, X. Guo, A. Nathan, All ink-jet printed low-voltage organic field-effect transistors on flexible substrate. *Org. Electron.* **2016**, *38,* 186–192.

This work demonstrates inkjet printed thin film transistor circuits on flexible substrates with the ability to heal themselves in real time from open faults. The healing mechanism is akin to how blood forms a clot in humans– i.e. the dispersed entities in blood rush to the site of injury and participate in healing. In this case, the active material is a dispersion of conductive particles in an insulating fluid. Self-healing is triggered by the electric field that appears in the open gap during the occurrence of the fault.

Li Ding, Pushkaraj Joshi, James Macdonald, Virendra Parab and Sanjiv Sambandan*

Self-Healing Thin Film Transistor Circuits on Flexible Substrates